JOURNAL OF CATALYSIS **173,** 257–267 (1998)
ARTICLE NO. CA971931

α-Alumina-Supported Nickel Catalysts Prepared from Nickel Acetylacetonate: A TPR Study

R. Molina and G. Poncelet[1]

Unité de Catalyse et Chimie des Matériaux Divisés, Université Catholique de Louvain, Place Croix du Sud 2/17, 1348 Louvain-la-Neuve, Belgium

Received December 5, 1996; revised September 29, 1997; accepted September 30, 1997

Supported Ni catalysts with low metal loadings prepared by impregnation of α-alumina with nickel acetylacetonate ($Ni(acac)_2$) have been studied by temperature-programmed reduction (TPR). The effect of the metal loading (between 0.4 and 1.7 wt%), washing and drying, and calcination temperature on the reduction profile, temperature of maximum reduction (T_M), and H_2/Ni ratio has been investigated. Metal–support interactions already exist at the impregnation step. The decomposition–reduction products of the organic moiety perturbing the TPR profiles and H_2 consumptions were suppressed when drying was done at 250°C. Two distinct metal species could be distinguished according to the calcination temperature. The one with T_M values $\leq$615°C occurred at calcination temperatures $\leq$400°C, whereas at 600°C and above, a second species was characterized by T_M values of 900°C and higher. The two species existed in different proportions in the solids calcined above 400°C and below 600°C. Some indication supported the formation of a nickel aluminate spinel-type phase when the solid was calcined at 600°C and above accounting for the high temperatures needed to reduce nickel oxide.

Key Words: **nickel acetylacetonate; α-alumina; TPR measurements.**

INTRODUCTION

The temperature-programmed reduction (TPR) technique eventually coupled with mass spectrometry has been extensively applied to the study of supported and unsupported metal catalysts, bimetallics, and alloys. Comprehensive reviews on the basic concepts and applications of the technique have been published (1, 2). Recently, Furlong *et al.* (3) have shown that TPR may also provide useful information on the removal of the organic ligands from organo–metal precursors.

The reduction of NiO/alumina and the effect of the experimental conditions on the catalytic properties of the reduced systems have been well documented (4–17). The more laborious reduction of NiO on alumina supports compared with bulk and silica-supported NiO has been ascribed to metal oxide–support interactions (8, 18, 19). Nonstoichiometric and stoichiometric nickel aluminate have been identified, in amounts and with structural characteristics depending on the preparation conditions (5, 8, 20). Incorporation of Al^{3+} into the surface layers of NiO during impregnation has also been evidenced (9, 21). Most of the studies on alumina-supported nickel oxide have been concerned with high-surface-area supports (mainly γ-alumina) and nickel loadings (ex nickel nitrate) higher than 5 wt%. At the opposite end, low-surface-area supports (α-alumina) and metal loadings below 5% have been much less addressed.

Supported Ni catalysts prepared with nickel acetylacetonate have been scarcely investigated, the little information available dealing mainly with catalytic reactions (22–25) and/or metal particle size measurements (26, 27). Fragmentary data on the decomposition of $Ni(acac)_2$/alumina prepared in the liquid phase were provided by van Veen *et al.* (28, 29). In more recent studies, the interactions between $Ni(acac)_2$ adsorbed in the gas phase on γ-alumina (30) and both γ-alumina and silica (31) have been investigated.

This study was devoted to $Ni(acac)_2/\alpha$-alumina catalytic systems with Ni loadings between 0.4 and 1.7 wt% in order to obtain information on the state of the catalyst at different steps of the preparation with respect to removal of the organic ligands from the nickel precursor, metal–support interaction, and effect of calcination temperature on the metal reducibility. Relations between reduction features, physicochemical and spectroscopic characterization, and catalytic activity will be treated in a separate article.

EXPERIMENTAL

Materials and Methods

A commercial α-alumina prepared by calcination of a transition alumina (from Rhone-Poulenc) was supplied by (former) Catalysts and Chemicals Europe. Its BET specific surface area and total pore volume (determined from N_2 sorption isotherm at 77 K with an ASAP-2000 sorptometer from Micromeritics on a sample outgassed for 4 h at 200°C) were 42 m^2/g and 0.21 cm^3/g, respectively. Microporosity was almost nonexistent. The X-ray diffraction (XRD)

[1] To whom correspondence should be addressed.

0021-9517/98 $25.00

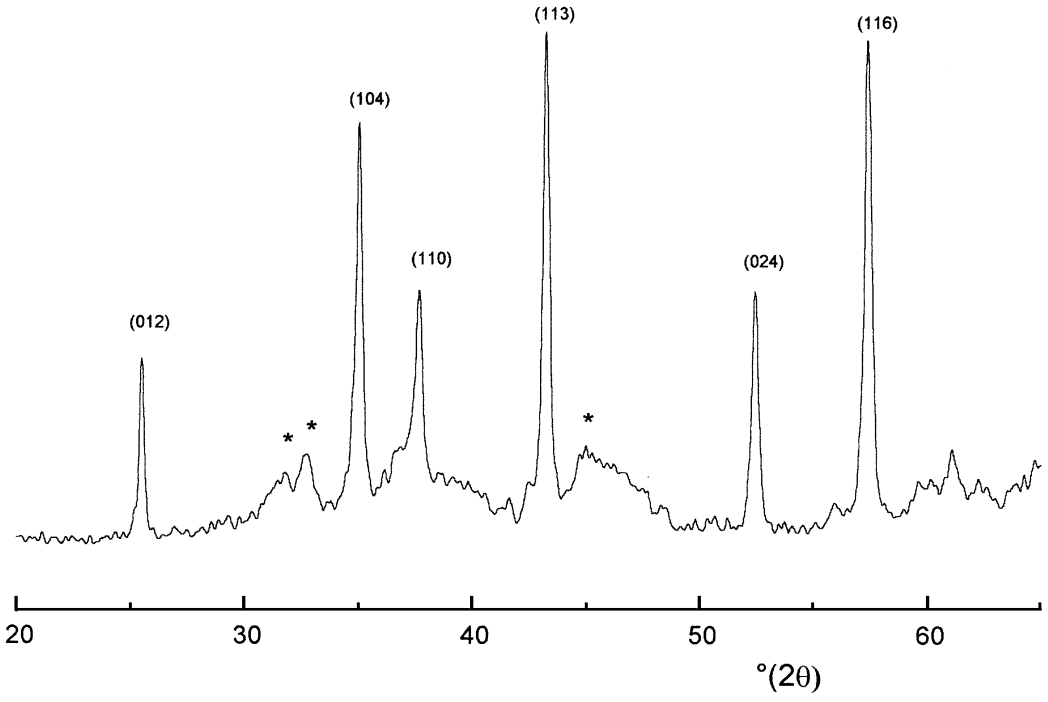

FIG. 1. X-ray diffraction pattern of the starting α-alumina. Peaks marked with ($*$) correspond to untransformed γ-alumina.

pattern of the starting support (Fig. 1) (recorded with a D-5000 Siemens instrument with copper anticathode) showed the narrow and intense reflections of α-alumina and a few broad and poorly defined peaks ascribed to small amounts of the parent γ-phase. It may be that these remnants contributed to the somewhat unusually high surface area, although α-aluminas with specific surface areas of 100 m^2/g and more have been mentioned in recent studies (32, 33). The surface hydroxyl density established from the weight loss between 500 and 1000°C was 1.28 OH nm^{-2}.

Nickel/alumina catalysts were prepared by adding the support (fraction $<100\ \mu$m precalcined at 500°C for 16 h) to a solution containing the required amount of nickel acetylacetonate (from Merck) dissolved in benzene (highest purity grade, from UCB). The solution was stirred for 15 min prior to the addition of the support. The slurry was stirred at room temperature for 48 h. After filtration, the solid was washed with pure benzene, dried between room temperature (4 h under vacuum) and 250°C (16 h), and calcined for 4 h at temperatures in the range 300–900°C. The metal content was established by inductively coupled plasma spectroscopy. NiO (analytical grade, from BDH) was used as a reference material and for the calibration of the TPR apparatus.

XPS analysis was carried out with a Vacuum Generators ESCA 3 MKII spectrometer equipped with a Tracor Northern TN1710 signal averager, and a Mg anode powered at 14 kV with a current beam of 24 mA and an Al window as the X-ray source.

TPR Measurements and Experimental Procedure

TPR experiments were carried out with a TPD/TPR 2705 instrument, 027 Pulse Chem Sorb option, from Micromeritics. The oven controller unit had a built-in circuit board and signal conditioning device which amplified the thermal conductivity detector (TCD) signal prior to sending it to a PC data acquisition system provided with a lab-developed programme. A chromel–alumel thermocouple was placed inside the quartz reactor which was fitted with capillary tubing at the outlet branch in order to increase the gas velocity and minimize the thermal gradient effects.

The reducing gas consisted of a H_2/Ar mixture [5 vol/vol% H_2 (99.99%)/95% Ar (99.996%) from Air Liquide]. Traces of oxygen and water were removed with "Oxy-trap" and "Hydro-purge," respectively (from Altech Associates). Argon was preferred over nitrogen as a diluent gas in order to avoid the possible formation of nitrides suspected by several authors (2, 34, 35). Water produced during the reduction was removed with a cold trap consisting of liquid nitrogen and isopropyl alcohol (down to -110°C). Duplicate experiments were performed using a TPR apparatus coupled with a mass spectrometer (TPR-MS) in order to identify the gaseous products formed during the reduction. In those runs, the cold trap was not used.

A weighed amount of sample was supported on a quartz wool plug inside the reactor. In order to avoid the effect of the operating variables on the shape of the TPR profile and temperature of maximum reduction (T_M), values of the

characteristic K and P numbers between 55 and 140 s, and $\leq$20 K, respectively, were calculated according to the empirical equations of Monti and Baiker (36) and Malet and Caballero (37), namely, $K = \mathrm{So}/V^*\mathrm{Co}$ and $P = \beta K$, where So is the amount of reducible species (in μmol), V^* is the total flow rate of the reducing gas mixture (in $\mathrm{cm^3(STP)s^{-1}}$), Co is the hydrogen concentration in the gas mixture (in $\mu\mathrm{mol\ cm^{-3}}$, and β is the heating rate (in $\mathrm{Ks^{-1}}$).

Prior to the TPR run, the sample was pretreated in flowing Ar for 1.5 h at the designated drying temperature and cooled to room temperature under Ar. The carrier gas was then switched to the reducing gas mixture while cooling the trap down. After stabilization of the TC detector, the temperature was linearly increased at a rate (β) of 0.17 $\mathrm{Ks^{-1}}$. All the experiments were carried out with a constant flow rate $V^* = 0.79$ $\mathrm{cm^3(STP)s^{-1}}$, and hydrogen concentration $\mathrm{Co} = 2.05$ $\mu\mathrm{mol\ cm^{-3}}$. TPR runs with the support (blank) and the support exposed to the same amount of solvent and drying conditions as those used at the impregnation step showed no H_2 uptake. Calibration of the equipment was done from the integrated area of the reduction profiles and the amounts of bulk NiO, a procedure which has proven to be more reliable and reproducible than the injection of hydrogen pulses in the carrier gas (34, 38). H_2 consumption was obtained from the integrated peak area relative to the calibration curve. The TPR profiles were normalized to the amount of nickel present. For a set of 15 measurements, the temperatures of maximum reduction (T_M) fluctuated between 370 and 390°C, with a standard deviation of 6.5°C (±1.7%) and average T_M of 382°C. H_2 consumptions were reproducible within ±2.6%. In establishing the calibration curve, complete reduction of nickel was assumed.

Absence of mass and heat transfer limitations (which may affect the reduction profile) was controlled with bulk NiO and $Ni(acac)_2$/alumina following the approaches of Monti and Baiker (36) and Fierro *et al.* (39) (mass transfer effects), and of Bosch *et al.* (35) (heat transfer limitations). In separate experiments, the Ni content of a same sample was analyzed before and after the TPR run, and after drying at 150°C and calcination at 900°C. No difference in the Ni content was observed, ruling out possible loss of metal by sublimation, another source of perturbation of the reduction profile (39).

RESULTS AND DISCUSSION

TPR of the Precursor

Before examining the reduction behavior of the $Ni(acac)_2/a\text{-}Al_2O_3$ systems, it is useful to look first at unsupported $Ni(acac)_2$ and $Hacac/Al_2O_3$ systems. The TPR profile of the dried precursor is often used as a signature to evaluate the degree of precursor–support interaction (21). $Ni(acac)_2$ showed a rather complex profile (Fig. 2a) attributable to reduction/decomposition processes of the organic moiety, the chemistry of which has been partly

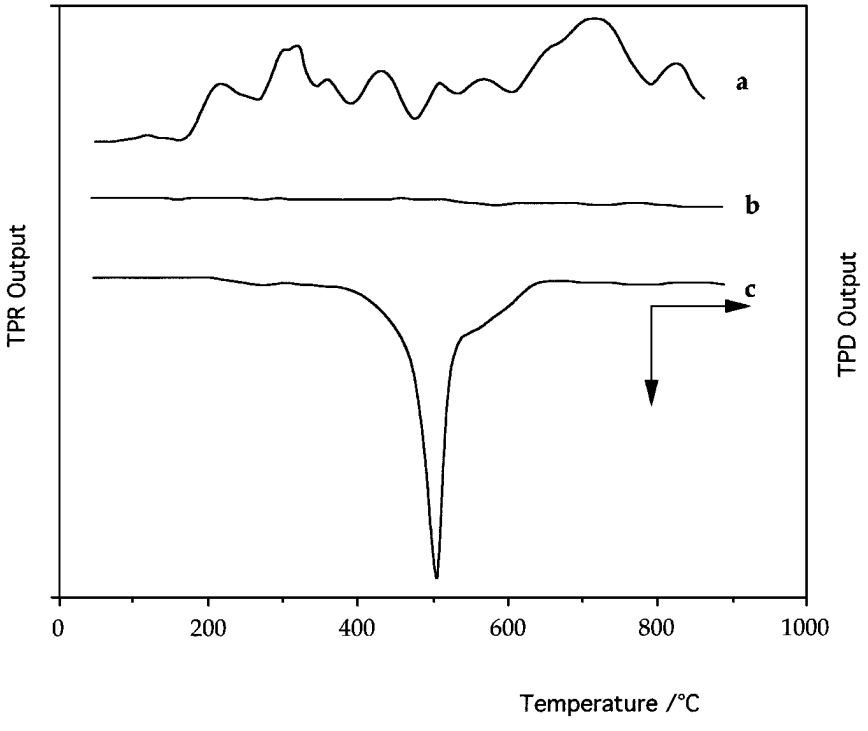

FIG. 2. TPR profiles of (a) $Ni(acac)_2$, (b) $H(acac)/\alpha\text{-}Al_2O_3$, and (c) TPD of $Ni(acac)_2/\alpha\text{-}Al_2O_3$.

clarified. In TPR-MS experiments, masses corresponding to H_2O^+, CO^+, CO_2^+, CH_3COCH^+, and $acac^+$ were identified in the outlet gases. When both TPR and TPR-MS were completed, the solid residue was totally black and a mirror of metallic nickel and yellowish green rings were deposited on the exit branch outside the heated zone. Thus, the complex signal probably represented the modifications of the gas-phase composition resulting from H_2 consumption/desorption and decomposition of the organic moiety to the different compounds mentioned. CH_4, which is formed by the reduction of acetone in the presence of a metallic phase (40), was not found in the reaction products.

The TPR of Hacac/α-Al_2O_3 (dried at 150°C overnight) showed no peak (Fig. 2b), but carbonaceous residues were noticed in the reactor at the end of the run. Mass spectroscopic analysis in a duplicate run indicated the presence of H_2O^+, $C_3H_5^+$, CO_2, acetone, and traces of unidentified compounds with masses of 91 and 105. As there was no H_2 consumption during the TPR, the small amount of water produced must come from the decomposition of acac. Similar compounds were also detected by van Veen *et al.* (28) in the case of Hacac/γ-alumina. The mass at 105 was attributed by these authors to a possible aromatic-derived compound. At the difference with our observation, no carbonaceous residue was found. On the basis of a multitechnique analysis, the authors proposed the following decomposition pathway:

$$|\mathrm{Al(acac)_2}|_\mathrm{s} \xrightarrow[\mathrm{H,OH}]{\Delta T} 2\,\mathrm{CH_3{-}CO{-}CH_3} + |\mathrm{Al(OAc)_2}|_\mathrm{s}$$

$$|\mathrm{Al(OAc)_2}|_\mathrm{s} \xrightarrow{\Delta T} \mathrm{CH_3{-}CO{-}CH_3} + \mathrm{CO_2} + |\mathrm{Al{-}O}|_\mathrm{s}.$$

Köhler *et al.* (41) found the same reaction products as in this study and proposed that metal acetylacetonates are partly decomposed by the catalytic action of the acidic and basic sites of the alumina surface involving the splitting of the acetylacetonate ligands and, possibly, the further transformation to acetone and acetic acid which strongly adsorb on Al^{+3} sites. In consecutive reactions, carbon oxides originating from the decomposition would form surface carbonates.

A TPD experiment with Ni(acac)$_2$/α-Al_2O_3 (1% Ni, dried at 150°C) done under conditions similar to those for TPR but in flowing pure argon showed a negative peak (Fig. 2c) at about the same temperature as that corresponding to the TPR signal. TPD-MS run over the same sample showed H_2O^+, mainly CO^+ and CO_2^+, and $acac^+$. As under TPD conditions no reduction is expected (absence of H_2 and metallic species), H_2O^+ probably originates from the decomposition of acac rather than from reduction of the system.

Effect of Washing

Obtainment of efficient catalysts requires one to relate their physicochemical and catalytic properties with the preparation conditions (26). In the dipping method (as in this work), mainly applied when the precursor interacts with the support, the metal loading is governed by the concentration of the adsorption sites at the support surface (42, 43), and washing with the pure solvent not only removes the excess of unreacted complex but also shifts the equilibrium toward the formation of surface species (44, 45). The following general reaction scheme for metal acetylacetonates adsorbing on alumina has been proposed by Van Der Voort *et al.* (46),

$$\mathrm{M(acac)}_x + |\mathrm{Al}|_\mathrm{s} \rightarrow |\mathrm{Al}|_\mathrm{s}{-}\mathrm{M} + x|\mathrm{Al}|_\mathrm{s}{-}\mathrm{acac},$$

where $|\mathrm{Al}|_\mathrm{s}$ stands for the alumina surface, without precisely defining the nature of the adsorption sites. For van Veen *et al.* (29), the reaction would occur via a ligand exchange mechanism, Hacac being adsorbed on the alumina surface. The adsorption sites may be acidic OH and basic groups, and coordinately unsaturated Al species, these latter ones constituting, according to these authors, the sites whereupon metal acetylacetonates exclusively react. Suntola (30) proposed a mechanism implying a reaction of Ni(acac)$_2$ with Al–O–H groups with the formation of =Al–O–Ni(acac), and H(acac) released in the gas phase, whereas Babich *et al.* (31) concluded that the nickel precursor is covalently bound to the support (γ-Al_2O_3 and SiO_2) as one acetylacetonate ligand of the precursor molecule substitutes with the oxygen atom of a surface hydroxyl group. The same authors proposed that acetylacetone evolving during the reaction reacts with coordinatively unsatured Al^{3+} ions of the support surface, resulting in the appearence of aluminium acetylacetonate surface species.

The possible adsorption sites of the alumina used in this study were investigated by infrared spectroscopy of adsorbed pyridine, ammonia, and CO_2. Both acid and basic sites were evidenced. In addition, ^{27}Al NMR spectra of the support revealed that about 17% of the aluminum was in fourfold coordination (signal at 63 ppm). In particular, diffuse reflectance IR spectroscopy (DRIFT) showed the suppression of the band at 3690 cm^{-1} of the support (OH groups) upon impregnation, suggesting their intervention in the interaction mechanism. These results will be detailed elsewhere.

Samples impregnated with Ni(acac)$_2$ were washed using 25 and 250 ml benzene/g. The Ni contents were not modified even after an exhaustive washing, which suggests that nickel–support interactions occurred right at the impregnation step and this is consistent with reported work on other metal acetylacetonates (46). Due to these interactions, the final distribution of the active phase is mainly determined at the impregnation step (42).

The different profiles of unsupported and supported Ni(acac)$_2$, the results obtained after exhaustive washing, and, as shown below, the products identified by mass spectrometry indicate that the precursor is modified when

TABLE 1

Effect of Ni Loadings and Drying Temperature

Drying temperature (°C)	Ni (wt%)	So (μmol Ni)	K (s)	T_M (°C)	H_2/Ni
150	1.7	139.7	89.4	469	1.8
150	1.0	151.8	94.0	478	1.7
150	0.8	113.0	69.9	502	2.3
150	0.4	103.3	63.9	542	2.0
200	1.7	144.4	89.4	534	1.1
200	1.0	172.2	106.6	550	1.1
200	0.8	125.9	78.0	563	0.8
200	0.4	91.8	57.0	505	0.7
250	1.7	101.4	62.8	537	0.9
250	1.0	151.8	94.0	571	1.1
250	0.8	126.1	78.1	592	0.7
250	0.4	90.6	56.1	662	0.4

supported on α-Al_2O_3, probably due to an interaction of the nickel precursor with the support. These observations could hardly be interpreted in terms of a simple precipitation of $Ni(acac)_2$ on the support (28, 29).

Influence of $Ni(acac)_2$ Loading

The experimental conditions, H_2/Ni molar ratios, and T_M values obtained from the reduction profiles of supported $Ni(acac)_2$ catalysts with various Ni loadings and dried at different temperatures are given in Table 1. Both parameters had an influence on the temperature of maximum reduction (T_M). For the samples dried at 150°C, the amount of hydrogen consumed during TPR corresponded to a H_2 : Ni stoichiometry higher than 1 : 1 which, as proposed by Furlong *et al.* (3) in the case of $Pd(acac)_2/\gamma$-alumina, would be due to a consumption of hydrogen for the reduction of the organic ligands. In addition, the gas-phase analysis in a duplicate TPR-MS run showed the presence of CH_4, CO, CO_2, and H_2O. Coq *et al.* (47) found CH_4 and CO_2 (and CH_3CO^+ at lower drying temperatures) under similar conditions and suggested as their probable origin the reduction of a carbonaceous compound present on the catalyst. Arnoldy and Moulijn (38) showed that reduction of acetone (identified in our TPR-MS runs with systems dried at lower temperatures) required H_2 consumption and resulted in the production of CH_4. The existence of a metallic phase (in the occurrence, Co) was a prerequisite for CH_4 formation. Our results are thus consistent as CH_4 was found for the $Ni(acac)_2/\alpha$-Al_2O_3 systems but not for unsupported $Ni(acac)_2$ and $Hacac/Al_2O_3$, nor in the TPD experiment over $Ni(acac)_2$/a-Al_2O_3. In addition, the formation of H_2O at this temperature indicated that reduction of nickel species also occurred.

For the samples dried at 200 and 250°C, H_2/Ni ratios were close to 1 at the higher metal loadings (1.0 and 1.7% Ni) and <1 for 0.4 and 0.8 wt% Ni, indicating incomplete reduction, and the tendency to lower stoichiometries at the low metal contents was more pronounced for the samples dried at 250°C. Uemura *et al.* (48) reported that low nickel-containing catalysts had a relatively large proportion of unreduced nickel which, upon migration, was stabilized at the vacancies of γ-alumina with defective spinel structure. Perhaps this interpretation could account for the $H_2/Ni < 1$ observed for the samples with low metal loadings. Mass spectroscopic analysis in a duplicate experiment with the sample containing 1% Ni dried at 250°C showed mostly water and only trace amounts of CH_4 and CO_2, pointing to the nearly complete removal at this temperature of the organic moiety adsorbed on the support surface. As suggested by several authors (46, 49, 50), the metal would be in its oxidized state, the oxygen probably being supplied by the surrounding air atmosphere, through a mechanism which still needs clarification. For Suntola (30), water vapor would be needed for the transformation of $=$Al–O–Ni(acac) to surface $=$Ni–O–H and removal of H(acac). At all drying temperatures, the reduction profiles broadened and the T_M values shifted to higher temperatures with decreasing metal content. This, together with the lower H/M ratios, stems from an increasing difficulty to reduce the metal species as illustrated in Fig. 3, where the T_M values have been plotted against the Ni loading at different drying temperatures. Reduction of Ni required increasing temperatures as the metal loading decreased, independent of the drying temperature. Similar trends reported for different systems have been interpreted in terms of stronger metal–support interactions (6, 34, 38, 51).

Influence of Calcination Temperature

The effect of calcination temperature on the reduction profile has been studied with 1.7% Ni catalysts dried at 250°C for 16 h under the following conditions: So = 144.4 μmol; $K = 89$ s; $P = 15$ K; calcination time = 4 h. The experimental results are given in Table 2 and the reduction

TABLE 2

Effect of Calcination Temperature (1.7% Ni/α-Al_2O_3)

T (°C)	T_M species I (°C)	T_M species II (°C)	H_2/Ni	Catalyst color
300	582	(839)	1.0	Light grey
350	604	(837)	1.0	Light grey
400	615	(836)	0.9	Light grey
450	671	835	1.1	Light grey-greenish
500	733	837	1.0	Pale greenish
600		905	0.8	Light blue
700		928	1.0	Light blue
900		990	<0.7	Greenish-light blue

Note. Conditions: So = 144.4 μmol; $K = 89$ s; $P = 15$ K; calcination time = 4 h; ( ), weak signals.

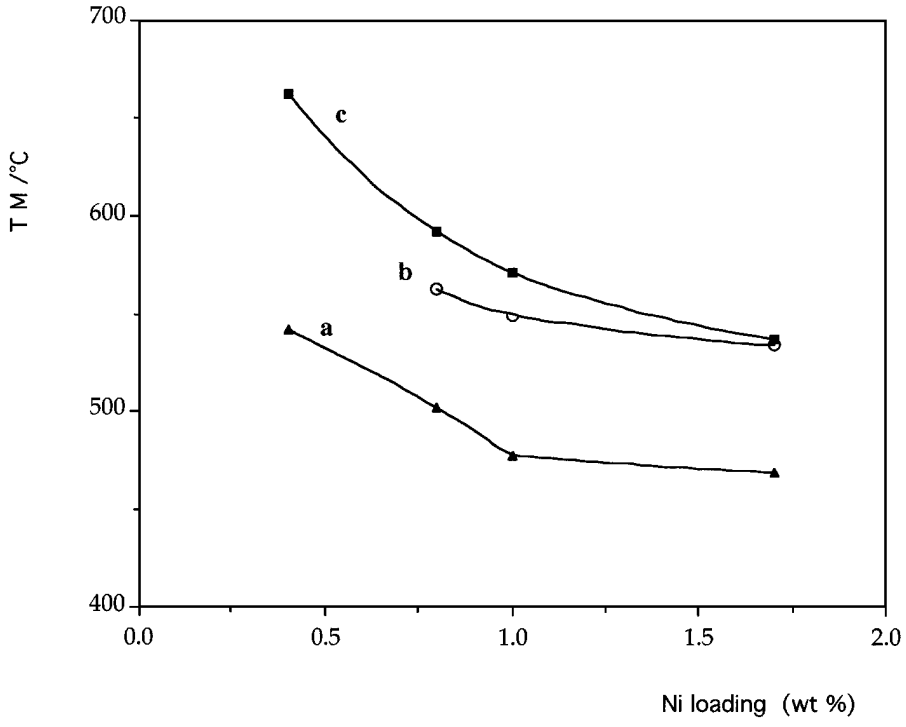

FIG. 3. Variation of T_M with nickel loading and drying temperature. (a) 150, (b) 200, and (c) 250°C.

profiles obtained after calcination between 300 and 900°C are shown in Fig. 4. Increasing calcination temperatures made the reduction increasingly more difficult as inferred from the continuous shift of the main reduction peak toward higher temperatures. Since Ni^{2+} is reduced to Ni^0 without going through intermediate oxides, the hydrogen consumption peaks appearing in different temperature regions are assigned to the reduction of different species (52, 53). The TPR profiles of the samples calcined at 450 and 500°C clearly show the simultaneous presence of two nickel species. In the following, species I will refer to the Ni species with T_M values lower than 750°C (calcination temperatures between 300 and 500°C), and species II will refer to a Ni species reduced above that temperature. In the samples calcined at 600°C and above, all the reducible nickel was of type II, a species which as well was increasingly more resistant to reduction (T_M values between 905 and 990°C depending on the calcination treatment). The relative proportions of the two species in the samples calcined at 450 and 500°C were estimated to be 72–28% (species I and II after calcination at 450°C) and 66–34% after calcination at 500°C, indicative of the progressive transformation of species I into species II. Sintering of Ni during reduction was observed by Bolt *et al.* (54) in the same range of temperatures. The T_M values of species I and II plotted, in Fig. 5, as a function of calcination temperature clearly show that the two species were differently affected (slope) by calcination temperature.

As indicated in Table 2, calcination at increasing temperatures was also accompanied by color changes of the solids. The samples calcined up to 500°C (corresponding to species I) were light grey to beige, whereas those calcined at 600°C and above (species II) clearly showed greenish to light blue coloration. A well-crystallized bulk $NiAl_2O_4$ prepared by calcining at 1200°C a stoichiometric mixture of the corresponding nitrates had a pronounced blue coloration and a T_M value slightly above 1100°C.

Increasing resistance to reduction with calcination temperature as found in this work has been reported by other authors, irrespective of the type of support (silica, alumina). Zielinski (8) found that NiO (ex-nitrate) was more difficult to reduce when supported over γ-alumina than over α-alumina. The opposite observation was reported by Medina *et al.* (55). If major differences in the reduction process result from the interactions between nickel oxide and high-surface-area supports (56, 57), decreased reducibility of nickel in NiO/Al_2O_3 catalysts with increasing calcination temperature has been accounted for by reinforced chemical interaction with the support, changes of the NiO crystallites size, and incorporation of mobile Al^{3+} (dissolved at the impregnation step) into NiO crystallites (9, 21), as well as by the formation of nonstoichiometric or stoichiometric nickel aluminate, in amounts and with structural organization (amorphous, crystalline) depending on the preparation conditions (6, 8, 15, 20, 38, 48, 58, 59).

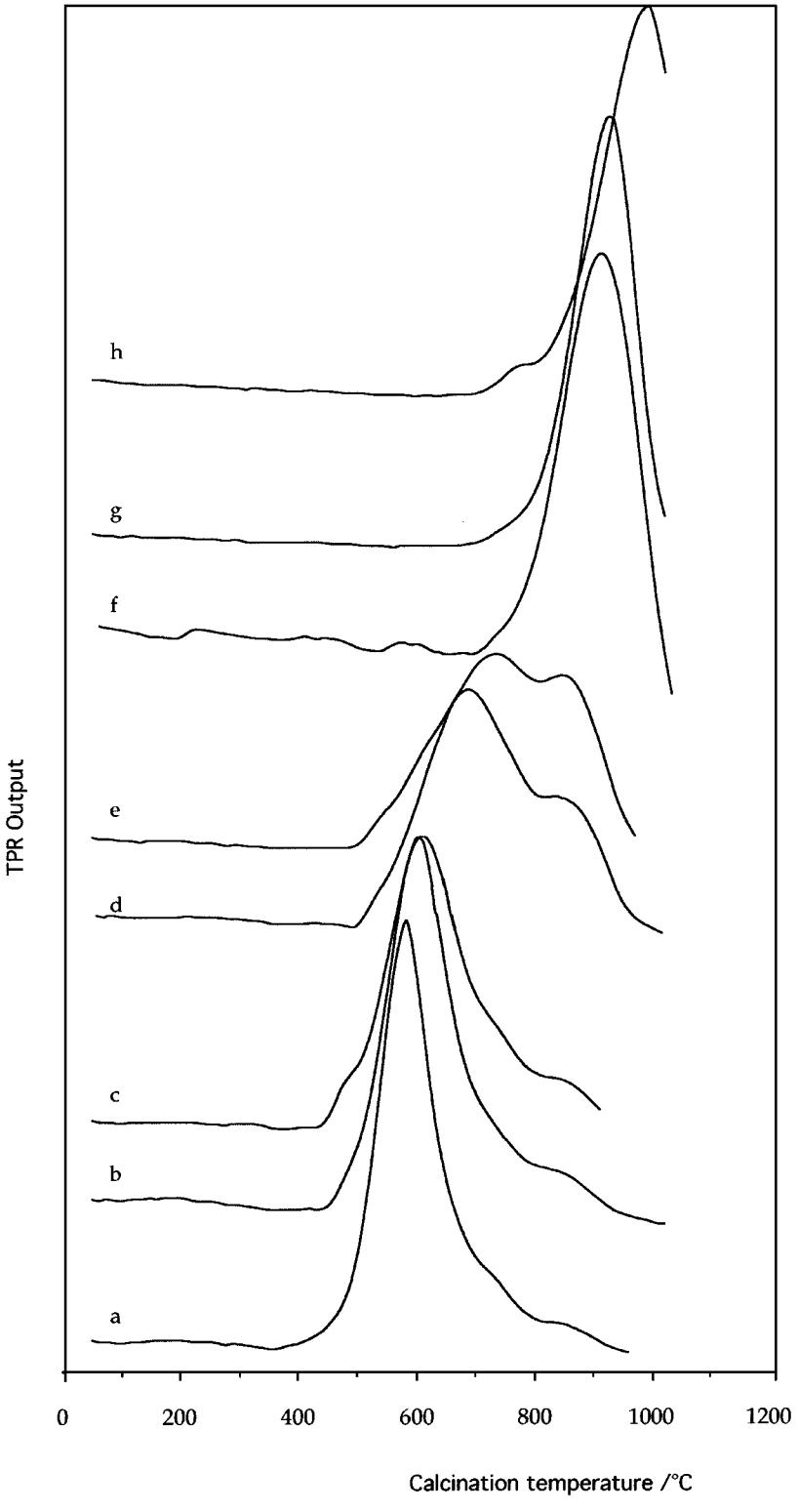

FIG. 4. Influence of the calcination temperature on the reduction profiles (1.7 wt% Ni). (a) 300, (b) 350, (c) 400, (d) 450, (e) 500, (f) 600, (g) 700, and (h) 900°C.

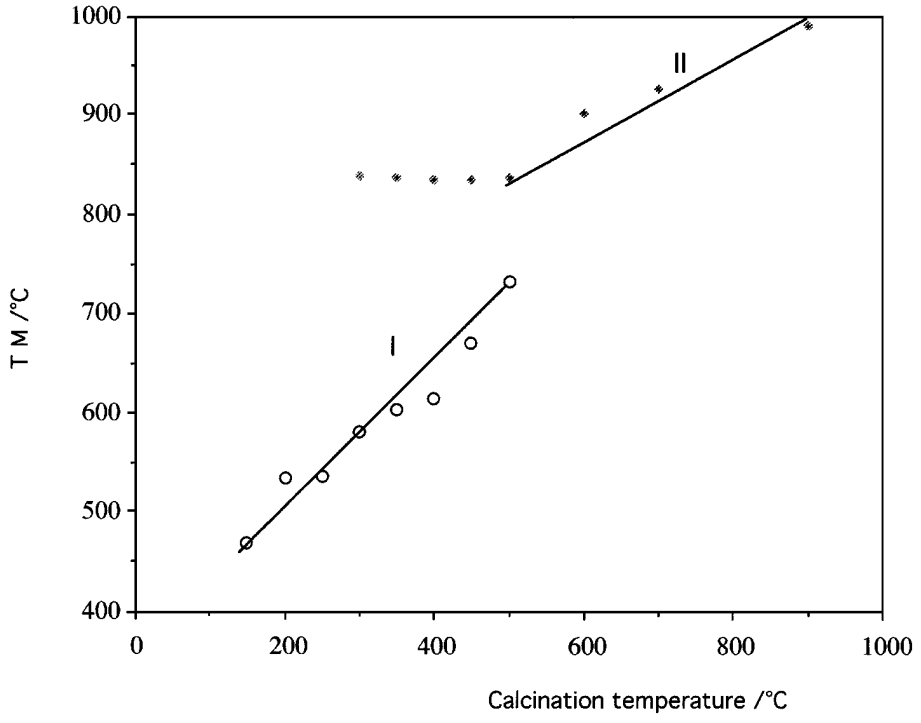

FIG. 5. Variation of T_M of species I and II with calcination temperature.

Zielinski (8) distinguished "free" NiO (not bound to alumina) with T_M near 230°C, and "fixed" NiO (as nickel aluminate) with T_M at 450°C. Scheffer *et al.* (52), investigating 2.0, 3.9, and 9.2% NiO/γ-Al_2O_3 catalysts, attributed the TPR peaks with T_M near 490 and 800°C of samples calcined at 400°C to highly dispersed, amorphous, surface Ni^{2+} species differing in reducibility due to the different number of Al^{3+} ions surrounding the Ni^{2+} ions (i.e., aluminium ions of the support inhibit the propagation of nucleation). For these authors, this calcination temperature (400°C) was too low for nickel ions to diffuse into γ-Al_2O_3, therefore excluding the formation of a spinel phase. A single peak with T_M at 850°C appearing in samples calcined at higher temperatures was assigned to a diluted $NiAl_2O_4$-like phase. Gavalas *et al.* (16) showed that NiO supported on α-Al_2O_3 (2.2% Ni) was not modified by a calcination below 500°C whereas above 850°C, a nickel aluminate precursor, insoluble in acid and hard to reduce, was formed. Lambert and Schulz-Ekloff (60) found evidence for NiO and $NiAl_2O_4$, with epitaxial growth of NiO crystallites for γ-alumina but not for α-alumina. Reduction between 500 and 700°C produced roughly spherical nickel crystallites surrounded by shells of nickel aluminate-type material. After reduction at 800°C, an increase of the lattice parameters of Ni on α-Al_2O_3 was noticed, suggesting incorporation of aluminium atoms into the structure.

Due to the small amounts of nickel used in this study and possibly also to its amorphous state, attempts to provide direct evidence for the formation of a spinel-like phase (possibly associated to the color changes) in the peripheral region of the support particles have failed. Detection of eventual modifications of the metal dispersion (or surface) with calcination temperature by XRD and room temperature hydrogen chemisorption (pulse and flow methods) was unsuccessful. The small hydrogen uptakes measured could be anticipated from the work of Bartholomew and Pannell (13), considering the low Ni loading (<3%) and the existence of strong metal–support interactions.

The TPR sequence presented in Fig. 4 shows qualitative similarities with that reported by Rynkowski *et al.* (6) for a 5 wt% NiO/γ-Al_2O_3 (ex nickel nitrate) with respect to the variation of the peak profiles, shift of T_M to higher values, and color changes of the solids with increasing calcination temperature, the main difference being that higher T_M values were found in this study. This is not surprising in view of the different nature of the nickel compound and support and in view of the fact that ample evidence exists in the literature that the properties of supported metal catalysts are not uniquely determined by the metal/support combination, but also depend on their preparation method and pretreatment conditions (5, 8, 13, 58). In the article referred to (6), reduction of Ni^{2+} species forming an amorphous phase (dominant in samples calcined between 300 and 550°C) occurred in the temperature range 575–660°C, whereas the spinel phase (formed at calcination temperatures higher than 550°C) was reduced above 690°C, with T_M values

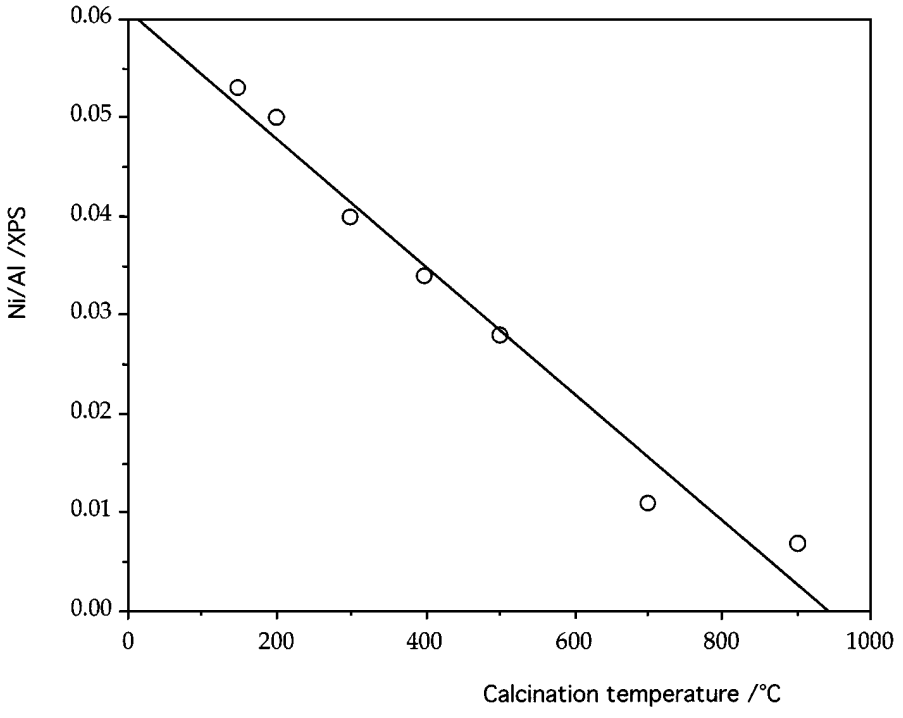

FIG. 6. XPS results: variation of surface Ni/Al ratio versus calcination temperature.

between 775 (calcination at 750°C) and 830°C (calcination at 900°C). No stoichiometric $NiAl_2O_4$ was identified by XRD, but merely a spinel in which Ni^{2+} ions were present in a diluted form.

Preliminary XPS results obtained on the calcined samples are shown in Fig. 6, where the surface Ni/Al ratios have been plotted against calcination temperature. Several interpretations may equally account for the decreasing relationship: sintering of NiO particles, migration (surface withdrawal) of Ni species into the support, surrounding of NiO crystallites by aluminium atoms (aluminium was found in the washing solvent). From the results of Figs. 4 to 6 on the one hand, and the similarity to the results of Rynkowski *et al.* (6) on the other hand, species I could be assigned to NiO interacting with (but not "chemically bound" to) the support. Indeed, the relatively high T_M values (in the range of 535 to 730°C for calcination temperatures between 300 and 500°C) compared with those found in the literature and the values obtained for unsupported NiO ($T_M = 382$°C) and for a 0.56 wt% Ni/α-alumina sample prepared by impregnation with nickel nitrate ($T_M = 380$°C) strongly point to the existence of interaction between the Ni species and the alumina support. Some sintering of nickel oxide in the samples calcined at 450 and 500°C may account for the shift of the T_M values of species I. Species II could be associated with the formation of a "nickel aluminate-type phase" (as suggested by the color changes of the calcined samples), more resistant to reduction (with T_M between 835 and 990°C), which would be in agreement with Rynkowski *et al.* (6).

It has been well established that small NiO particles are less reducible than bulkier NiO, a result which has been ascribed to the low rate of nucleation in the smaller particles (61–63). This may partly explain the higher temperatures needed for the reduction of the $Ni(acac)_2$ systems compared with similar catalysts prepared from nickel nitrate, especially for the Ni species I in which particles of the order of 50 Å were observed by transmission electron microscopy (sample with 1.7% Ni calcined at 300°C). The same sample calcined at 900°C showed NiO particles with estimated diameter of 500 Å, which goes in the opposite way if this parameter was playing a role on the reducibility. It seems thus that the first explanation, supported by a recent work of Li and Chen (63), is the most reasonable one. Finally, a possible limited migration of Al in or onto the NiO particles (9, 21) cannot be excluded. Small amounts of aluminum were found in the benzene collected at the washing step. It may be assumed that some mobile Al could exist on the support surface and migrate as calcination temperature increased, which would as well make the reduction increasingly more difficult (52). Further refined analysis and deconvolution of the XPS Ni 1*s* signals are in progress in order to establish whether the Ni species I and II can be discriminated (64).

CONCLUSION

Supported nickel catalysts have been prepared by impregnation of α-alumina with $Ni(acac)_2$. Interaction between

support and metal precursor occurred at the impregnation step. Low drying temperatures were found to affect the TPR profile and hydrogen consumption, mainly due to the contribution of decomposition/reduction products of the organic moiety superimposing with the reduction of the metal species. This interference was suppressed after drying at 250°C and above. Reduction of nickel in catalysts with low metal loadings (<1 wt%) needed higher temperature than those with higher metal contents (1.7 wt%), regardless of the temperature of the drying step, and the tendency for incomplete reduction increased with decreasing metal loadings. An enhancement of the calcination temperature shifted the T_M values to higher temperatures. Two types of metal species could be distinguished. The first one, with T_M values increasing from 534 to 733°C, was observed for catalysts calcined between 300 and 400°C. In samples calcined at 600°C and above, all the nickel was transformed into another species with T_M values going from 835 to 990°C, reflecting an increasing resistance to reduction. At calcination temperatures between 450 and 500°C, the two Ni species coexisted in different proportions. The similarity to literature data (high T_M values, color changes with calcination temperature) and the decreasing Ni/Al XPS surface ratios with increasing calcination temperature suggested the progressive formation of a "nickel aluminate spinel-type" phase. However, a possible limited insertion of mobile surface Al species into the nickel oxide particles could account to some extent for the results.

ACKNOWLEDGMENTS

R.M. is indebted to Colciencias, Colombia, for a doctoral grant. The authors gratefully acknowledge the Fonds National de la Recherche Scientifique, Belgium, for financing the TPR equipment as well as Professor P. Grobet (Centrum voor Oppervlaktechemie and Katalyse, Katholieke Universiteit Leuven) for the NMR data, and Professor J. Barrault (ESIP, University of Poitiers) for the TEM examination.

REFERENCES

1. Hurst, N. W., Gentry, S. J., Jones, A., and McNicol, B. D., *Catal. Rev. Sci. Eng.* **24**, 233 (1982).
2. Jones, A., and McNicol, B. D., *in* "Temperature-Programmed Reduction for Solid Materials Characterization," Chemical Industries, Vol. 24, Dekker, New York, 1986.
3. Furlong, B. K., Hightower, J. W., Chan, T. Y. L., Sarkany, A., and Guczi, L., *Appl. Catal.* **117**, 41 (1994).
4. Bartholomew, C. H., Pannell, R. B., and Fowler, R. W., *J. Catal.* **79**, 34 (1983).
5. Hu, J., and Schwarz, J. A., *Appl. Catal.* **51**, 223 (1989).
6. Rynkowski, J. M., Paryjczal, T., and Lenik, M., *Appl. Catal.* **106**, 73 (1993).
7. Turlier, P., Praliaud, H., Moral, P., Martin, G. A., and Dalmon, J. A., *Appl. Catal.* **19**, 287 (1985).
8. Zielinski, J., *J. Catal.* **76**, 157 (1982).
9. Richardson, J. T., Lei, M., Turk, B., Forster, K., and Twigg, M. V., *Appl. Catal.* **110**, 217 (1994).
10. Brown, R., Cooper, M. E., and Whan, D. A., *Appl. Catal.* **3**, 177 (1982).
11. Reinen, D., and Selwood, P. W., *J. Catal.* **2**, 109 (1963).
12. Bartholomew, C. D., and Ferrauto, R. J., *J. Catal.* **45**, 41 (1976).
13. Bartholomew, C. D., and Pannell, R. B., *J. Catal.* **65**, 390 (1980).
14. Vedrine, J. C., Hollinger, G., and Duc, T. M., *J. Phys. Chem.* **82**, 1515 (1978).
15. Houalla, M., Lemaître, J., and Delmon, B., *J. Chem. Soc. Faraday Trans.* **78**, 1389 (1982).
16. Gavalas, G. R., Phichitkul, C., and Voecks, G. E., *J. Catal.* **88**, 54 (1984).
17. Gandia, L. M., and Montes, M., *J. Mol. Catal.* **94**, 347 (1994).
18. Roman, A., and Delmon, B., *J. Catal.* **30**, 333 (1973).
19. Parysczak, T., Rynkowki, J., and Krzyzanowki, V., *React. Kinet. Catal. Lett.* **21**, 295 (1982).
20. Vorobev, W. M., *Kinet. Catal.* **16**, 215 (1976); **17**, 208 (1976).
21. Chen, S. L., Zhang, H. L., Hu, J., Contescu, C., and Schwarz, J. A., *Appl. Catal.* **73**, 289 (1991).
22. Tkach, V. S., Schmidt, F. K., and Sergeva, T. N., *Kinet. Katal.* **17**, 208 (1974).
23. Boulhel, E., Lazslo, P., Levart, M., Montaufier, M.-T., and Singh, G. P., *Tetrahedr. Lett.* **34**, 1123 (1993).
24. Angelescu, E., Stanescu, R., Parvulescu, V., Botez, L., and Angelescu, A., *Progr. Catal.* **1**, 24 (1993).
25. Molina, R., and Poncelet, G., *in* "XIV Simp. Iber. Amer. Catal., Chile," Vol. 1, p. 253, Soc. Chilena Quimica, 1994.
26. Uemura, Y., Hatate, Y., and Ikari, A., *J. Chem. Eng. Japan* **20**, 563 (1987).
27. Takayasu, O., Hata, T., and Matsuura, I., *Chem. Express* **5**, 829 (1990).
28. van Veen, J. A. R., de Jong-Versloot, P. C., van Kessel, G. M. M., and Fels, F. J., *Thermochim. Acta* **152**, 359 (1989).
29. van Veen, J. A. R., Jonkers, G., and Hesselink, W. H., *J. Chem. Soc. Faraday Trans.* **85**, 389 (1989).
30. Suntola, T., *Appl. Surf. Sci.* **100–101**, 391 (1996).
31. Babich, I. V., Plyuto, Y. V., Van Langenveld, A. D., Moulijn, J. A., and Vansant, E., *Appl. Surf. Sci.* **115**, 267 (1997).
32. Mao, C. F., and Vannice, M. A., *Appl. Catal.* **111**, 151 (1994).
33. McCabe, R. W., Usmer, R. K., Ober, K., and Gandhi, H. S., *J. Catal.* **151**, 389 (1995).
34. Rajagopal, S., Marini, H. J., Marzari, J. A., and Miranda, R., *J. Catal.* **147**, 417 (1994).
35. Bosch, H., Kip, B. J., van Ommen, J. G., and Gellings, P. J., *J. Chem. Soc. Faraday Trans.* **80**, 2479 (1984).
36. Monti, D. A. M., and Baiker, A., *J. Catal.* **83**, 323 (1983).
37. Malet, P., and Caballero, A., *J. Chem. Soc. Faraday Trans.* **84**, 2369 (1988).
38. Mile, B., Stirling, D., Zammitt, M. A., Lovell, A., and Webb, M., *J. Catal.* **114**, 217 (1988).
39. Fierro, G., Lo Jacono, M., Inversi, M., Porta, P., Lavecchia, R., and Cioci, F., *J. Catal.* **148**, 709 (1994).
40. Arnoldy, P., and Moulijn, J. A., *J. Catal.* **93**, 38 (1985).
41. Köhler, S., Reiche, M., Frobel, C., and Baerns, M., *in* "Studies in Surface Science and Catalysis," Vol. 91, p. 1009, Elsevier, Amsterdam, 1995.
42. Foger, K., *in* "Catalysis, Science and Technology" (J. R. Anderson and M. Boudart, Eds.), Vol. 6, p. 227, Springer-Verlag, Berlin/New York, 1984.
43. Marcilly, C., and Françk, J. P., *Rev. Inst. Franç. du Pétrole* **39**, 337 (1984).
44. Agostini, G., Ledoux, M. J., Hilaire, L., and Maire, G., *in* "Studies in Surface Science and Catalysis," Vol. 31, p. 569, Elsevier, Amsterdam, 1987.
45. Klimov, O. V., Fedotov, M. A., and Startsev, N., *J. Catal.* **139**, 142 (1993).
46. Van Der Voort, P., Babitch, I. V., Grobet, P. J., Verberckmoes, A. A., and Vansant, E. F., *J. Chem. Soc. Faraday Trans.* **92**, 3635 (1996).
47. Coq, B., Crabb, E., Warawdekar, M., Bond, G. C., Slaa, J. C., Galvagno, S., Mercadante, L., Ruiz, J. G., and Sanchez Sierra, M. C., *J. Mol. Catal.* **92**, 107 (1994).
48. Uemura, Y., Hatate, Y., and Ikari, A., *Sekiyu Gakkaishi* **29**, 143 (1987).

49. Kenvin, J. C., White, M. G., and Mitchell, M. B., *Langmuir* **7**, 1198 (1991).
50. White, M. G., *Catal. Today* **18**, 73 (1993).
51. Brito, J. L., and Laine, J., *J. Catal.* **139**, 540 (1993).
52. Scheffer, B., Molhoek, P., and Moulijn, J. A., *Appl. Catal.* **46**, 11 (1989).
53. Hu, C.-W., Yao, J., Yang, H.-Q., Chen, Y., and Tian, A.-M., *J. Catal.* **166**, 1 (1997).
54. Bolt, P. H., Habraken, F. H. P., and Geus, J. W., *J. Catal.* **151**, 300 (1995).
55. Medina, F., Salagre, P., and Sueiras, J.-E., *J. Chem. Soc. Faraday Trans.* **90**, 1455 (1994).
56. Montes, M., Soupart, J. B., De Saedeleer, M., Hodnett, B. K., and Delmon, B., *J. Chem. Soc. Faraday Trans.* **80**, 3209 (1984).
57. Boldyrev, V. V., Bulens, M., and Delmon, B., *in* "Studies in Surface Science and Catalysis," Vol. 2, Elsevier, Amsterdam, 1979.
58. Coenen, J. W. E., *in* "Studies in Surface Science and Catalysis," Vol. 3, p. 89, Elsevier, Amsterdam, 1979.
59. Lo Jacono, M., Schiavello, M., and Cimino, A., *J. Phys. Chem.* **75**, 1044 (1971).
60. Lambert, R., and Schulz-Ekloff, G., *Surf. Sci.* **258**, 107 (1991).
61. Houalla, M., Delannay, F., and Delmon, B., *J. Chem. Soc. Faraday Trans.* **76**, 2128 (1980).
62. Ho, S. C., and Chou, T. S., *Ind. Eng. Chem. Res.* **34**, 2279 (1995).
63. Li, C. H., and Chen, Y. W., *Thermochim. Acta* **256**, 457 (1995).
64. Molina, R., and Poncelet, G., in preparation.